Geomorphology 462 (2024) 109330

Contents lists available at ScienceDirect

Geomorphology

journal homepage: www.journals.elsevier.com/geomorphology

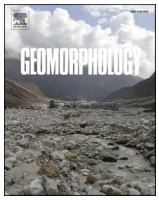

New data on tributary terraces and a reappraisal of the incision history of the Jinshan Gorge, middle Yellow River

Yuezhi Zhong [a,*], Vincenzo Picotti [a], Jianguo Xiong [b], Sean D. Willett [a], Christoph Schmidt [c], Georgina King [c]

[a] Department of Earth Sciences, ETH Zurich, Sonneggstrasse 5, 8092 Zurich, Switzerland
[b] State Key Laboratory of Earthquake Dynamics, Institute of Geology, China Earthquake Administration, Beijing 100029, China
[c] Institute of Earth Surface Dynamics, University of Lausanne, Bâtiment Géopolis, 1015 Lausanne, Switzerland

ARTICLE INFO

Keywords:
Tributary terraces
Jinshan Gorge
Incision history
Middle Yellow River

ABSTRACT

River channel profiles and river terraces are two typical landscape features to investigate river incision history. However, incision history inferred from the two markers can be inconsistent. For example, along the Jinshan Gorge in the middle Yellow River, pseudo-terraces (a virtual metric derived from channel profile modelling) suggest a recent acceleration in incision rates only in the southern gorge, and the northern keeps steady, while river terraces in the trunk channel indicate recently increased incision rates all along the gorge. To mitigate these discrepancies, we investigate six tributaries along the Jinshan Gorge by mapping and dating several strath terraces at various distances from the confluence to the trunk channel. By comparing tributary terraces of similar age, we find generally increasing incision rates towards the confluence with the trunk river in the southern Jinshan Gorge. North to south increasing incision rates along the gorge are also observed from coeval tributary terraces. In addition, two different landscapes between the southern and northern tributaries near the confluence are recognized, one with a deeply incised gorge and another one with floodplains, suggesting incision rate in the northern gorge is steady through time. Integrating the new infrared stimulated luminescence (IRSL) and Accelerator Mass Spectrometry (AMS) ^{14}C data from tributaries with the abundant literature data of terrace samples mostly in the Jinshan Gorge dated with various methods, we suggest published ages from optically stimulated luminescence (OSL) might be too young. The methodological limitation associated to the dating method can explain the observed mismatch of incision history in the northern gorge inferred from pseudo-terraces and from river terraces in the trunk channel, and reconcile some contradicting patterns in published trunk terrace data.

1. Introduction

Rivers are one of the major agents changing the Earth's surface and evolve dynamically through time in response to climate fluctuations and/or tectonic activities (e.g. Rhoads, 2020). River terraces and river longitudinal profiles are two common geomorphic markers to investigate the incision history of a bedrock river. Constrained strath height and formation age of terrace have been utilized to estimate the mean vertical incision rate and its temporal variations along river (Burbank and Anderson, 2011). Analysis of bedrock channel networks linking the bedrock erosion to stream power law also provides information on river incision history (Pazzaglia et al., 1998) in time (Roberts and White, 2010; Goren et al., 2014) or in space and time (Fox et al., 2014). Although river incision history reconstructed from river profiles is assumed to be consistent with terrace-based measurements (e.g. Merritts et al., 1994; Pazzaglia et al., 1998), discrepancies still arise, for example, in the middle Yellow River (Zhong et al., 2022).

The Yellow River in China (Fig. 1A) is one of the longest rivers in the world. The Jinshan Gorge in the middle Yellow River represents the ~700 km reach that connects the Weihe and Hetao Grabens. Several studies hypothesized that the connection recently occurred (Pan et al., 2012; Liang et al., 2015; Hu et al., 2016). However, different hypotheses about when and how the integration occurred exist: The time for integration of the Yellow River and development of the Jinshan Gorge has been proposed to be the late Miocene-early Pliocene (Lin et al., 2001), between 3.7 and 1.2 Ma (Pan et al., 2012), or after 0.25 Ma (Liang et al.,

* Corresponding author.
E-mail address: 1401214641@pku.edu.cn (Y. Zhong).

https://doi.org/10.1016/j.geomorph.2024.109330
Received 19 January 2024; Received in revised form 2 July 2024; Accepted 2 July 2024
Available online 5 July 2024

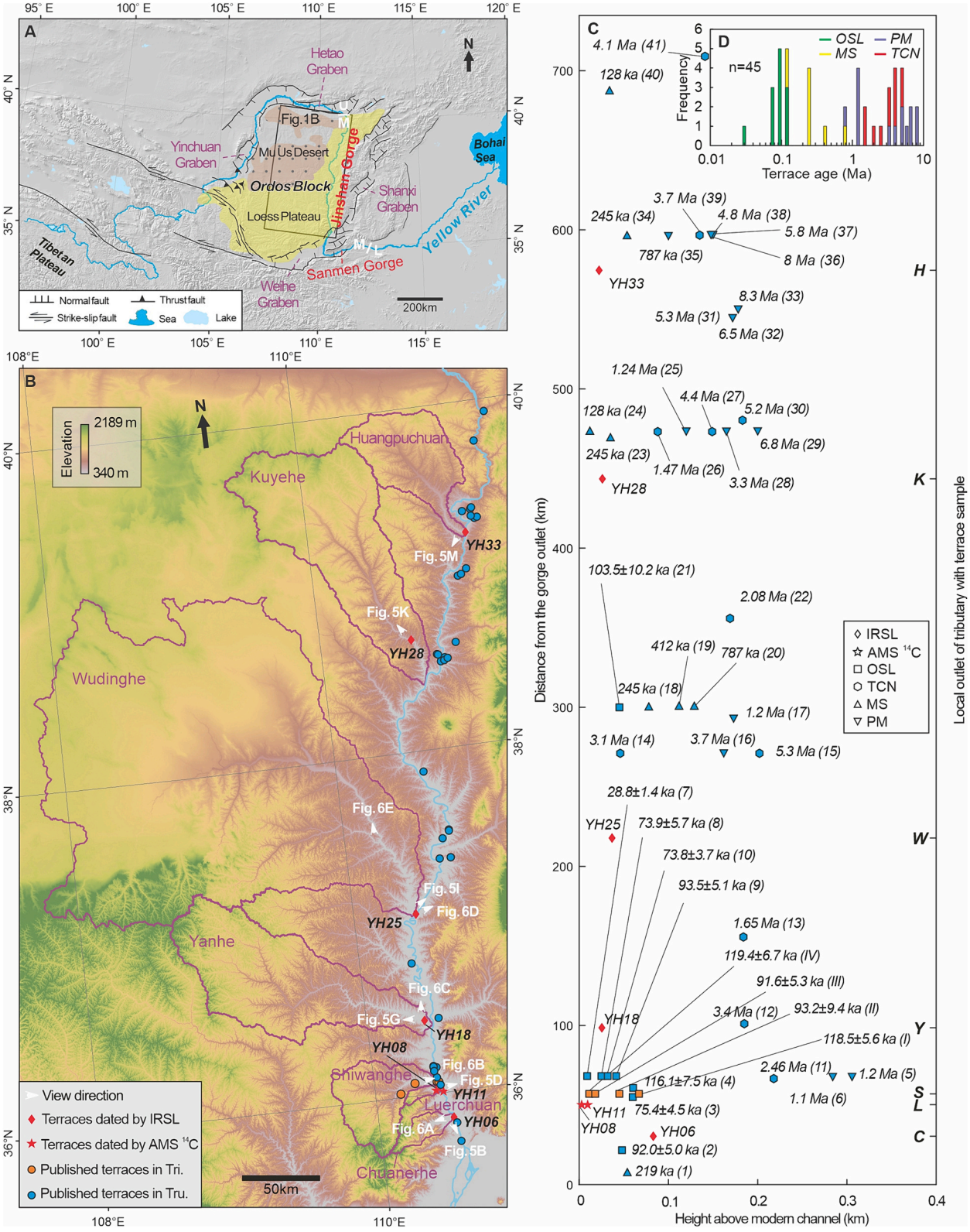

Fig. 1. Topography, active tectonics, dating sample distributions and extents of tributaries with dated fluvial terraces along the Jinshan Gorge. **(A)** Major faults around the study area. The Yellow River's main channel shown in blue lines and divided into upper (U), middle (M) and lower (L) reaches. **(B)** The locations of new terrace samples in this study and published terrace samples in the area. Topographic map derived from Shuttle Radar Topography Mission (SRTM) image. Drainage extent of tributaries with terrace samples shown with white lines. **(C)** Terrace heights and ages along the Jinshan Gorge, markers in brackets show samples' ID in Table 1. Letter in bold on the right axis is the initial of a tributary's name. **(D)** Histogram of published terrace ages in tributaries and trunk channel along the Jinshan Gorge. Colors show different dating methods. OSL: optically stimulated luminescence; MS: magnetic susceptibility; PM: paleomagnetism; TCN: terrestrial cosmogenic nuclides; IRSL: infrared stimulated luminescence. The figure is modified from Zhong et al. (2022).

2015). Reasons for the integration have been suggested as tectonic uplift and rifting (Lin et al., 2001), paleolake regression (Liang et al., 2015; Hu et al., 2017) or sea level fluctuations (Xiao et al., 2020). These debates attract widespread attention to the incision history of the Jinshan Gorge, which provides important information on integration of the Yellow River as well as related possible tectonic and/or climatic drivers.

Terraces in the trunk channel within the Jinshan Gorge have been extensively investigated in recent decades (Wang, 2006; Guo et al., 2012; Pan et al., 2012; Liang et al., 2015; Hu et al., 2016; Liang, 2017; Liu, 2020; Li et al., 2021) (Fig. 1, Table 1). With published terrace samples distributed at ~70 km, ~300 km, ~480 km and ~ 600 km upstream from the gorge outlet (Fig. 1B, C and Table 1), recent acceleration in incision rates since ~100 ka or ~ 250 ka are indicated, and some studies suggested the rapid incision all along the gorge as an indicator of the recent full integration of the Yellow River (Qiu et al., 2014; Liang et al., 2015). However, based on pseudo-terraces, i.e., artificial geomorphic markers created from an inversion analysis of tributary channel profiles that provide information on the incision history of the trunk channel (Zhong et al., 2022), only the southern gorge shows a recent increase of river incision, whereas more uniform and steady incision rates are indicated in the northern gorge.

In this paper, we intend to explore potential reasons for these discrepancies in the incision history reconstructed through river terraces and pseudo-terraces, aiming, for one thing, to better understand the regional history of incision and integration in the middle Yellow River, and for another, to assess the applicability of the theoretical approach of the river profiles that is widely applied in modern river geomorphology (e.g. Kirby and Whipple, 2012) to reconstruct bedrock river incision history. To these goals, we present new records of the late Quaternary fluvial terraces in six tributaries along the gorge (Fig. 1B), and discuss them within the frame of the pre-existing terrace data along the Jinshan Gorge. The timing of terrace formation is constrained with IRSL measurements and AMS radiocarbon dating. We quantify the incision amount since terrace formation by measuring the strath height above the modern channel.

2. Regional background

2.1. Geologic background

The Jinshan Gorge is located in the Ordos Block with little evidence of interior deformation (Shi et al., 2020) (Fig. 1A). The Ordos Block was formerly an intracontinental basin with generally the same lithostratigraphic units and depositional environment, dominated by alluvial and lacustrine processes (e.g. Ritts et al., 2009; Clinkscales et al., 2021) (Fig. 2A). In the Middle Jurassic to Early Cretaceous, the Ordos Basin experienced its last period of subsidence prior to undergoing partial inversion and dissection and is thought to have been tectonically stable since the end of the Mesozoic (e.g. Ritts et al., 2009; Xiong and Tang, 2019). In contrast to this, during the Paleogene the Ordos Basin bounding faults were reactivated to form narrow graben systems, presently fringing the former interior of the basin (Ritts et al., 2009) (Fig. 1A). This latter wide area represents the so-called stable Ordos Block (Ritts et al., 2009; Shi et al., 2020). The block is widely capped by Neogene red clay and thick Quaternary loess deposits with variable thickness, on average ~ 100 m (Liu, 1985; Xiong and Tang, 2019). Fluvial channels are well developed on the block, especially along the Jinshan Gorge, and drainage basins show little network reorganization (Willett et al., 2014). These channels are not only eroded through the thick aeolian deposits, but also incised into the bedrock, exposing underlying Permo-Mesozoic units (Fig. 2A).

Climate conditions around the Jinshan Gorge are dominated by the East Asian Monsoon, with about 70 % of its annual precipitation in the summer (Li et al., 2017). Annual mean precipitation gradually decreases from southeast (~600 mm/a) to northwest (<200 mm/a) (Fig. 2B).

The Ordos Block landscape is characterized by a highly dissected

Table 1
Published terrace data in tributaries and the trunk channel along the Jinshan Gorge.

ID	Longitude	Latitude	Strath [m]	Age [ka]	Predicted t * [m]	Method
1(Liang, 2017)	110° 34.43′	35° 42.36′	54	219	1364	MS
2(Liang, 2017)	110° 33.73′	35° 49.46′	48	92.0 ± 5.0	960	OSL
3(Liang, 2017)	110° 28.67′	36° 03.39′	60	75.4 ± 4.5	754	OSL
4(Guo et al., 2012)	110° 27.46′	36° 06.26′	60	116.1 ± 7.5	735	OSL
5(Hu et al., 2016)	110° 27.00′	36° 09.00′	306	1200	5171	PM
6(Hu et al., 2016)	110° 27.58′	36° 09.33′	284	1100	4628	PM
7(Zhang et al., 2011)	110° 26.25′	36° 09.75′	9	28.8 ± 1.4	106	OSL
8(Guo et al., 2012)	110° 26.23′	36° 09.77′	25	73.9 ± 5.7	298	OSL
9(Guo et al., 2012)	110° 26.33′	36° 10.00′	41	93.5 ± 5.1	495	OSL
10(Liang, 2017)	110° 26.30′	36° 10.36′	32	73.8 ± 3.7	383	OSL
11(Li et al., 2020)	110° 26.30′	36° 07.91′	218	2460	3111	TCN
12(Li et al., 2021)	110° 31.21′	36° 26.29′	185	3400	3163	TCN
13(Li et al., 2020)	110° 22.47′	36° 46.48′	184	1650	3588	TCN
14(Li et al., 2021)	110° 40.53′	37° 21.75′	46	3100	1098	TCN
15(Li et al., 2021)	110° 45.51′	37° 21.71′	202	5300	5342	TCN
16(Liu, 2020)	110° 45.51′	37° 21.71′	162	3700	3972	PM
17(Pan et al., 2012)	110° 43.32′	37° 28.65′	173	1200	5426	PM
18(Hu et al., 2016)	110° 46.54′	37° 31.37′	78	245	2536	MS
19(Hu et al., 2016)	110° 46.54′	37° 31.37′	112	412	3562	MS
20(Hu et al., 2016)	110° 46.54′	37° 31.37′	129	787	4022	MS
21(Hu et al., 2016)	110° 46.54′	37° 31.37′	45	103.5 ± 10.2	1290	OSL
22(Li et al., 2020)	110° 38.52′	37° 52.73′	169	2080	4312	TCN
23(Cao, 2012)	110° 53.10′	38° 30.33′	35	245	1376	MS
24(Cao, 2012)	110° 54.60′	38° 31.37′	12	128	427	MS
25(Cao, 2012)	110° 54.95′	38° 31.62′	120	1240	4219	PM
26(Li et al., 2020)	110° 54.17′	38° 30.67′	88	1470	3230	TCN

(continued on next page)

Table 1 (*continued*)

ID	Longitude	Latitude	Strath [m]	Age [ka]	Predicted t * [m]	Method
27(Li et al., 2021)	110° 51.59′	38° 32.80′	149	4400	4934	TCN
28 (Liu et al., 2007)	110° 55.80′	38° 31.20′	165	3300	5367	PM
29(Liu, 2014)	110° 51.00′	38° 33.00′	200	6800	6624	PM
30(Li et al., 2021)	111° 00.29′	38° 36.45′	183	5200	5752	TCN
31(Liu, 2020)	111° 05.15′	38° 59.33′	172	5300	7655	PM
32(Liu, 2020)	111° 06.68′	38° 59.78′	172	6500	7655	PM
33(Liu, 2020)	111° 09.36′	39° 01.55′	178	8300	8303	PM
34(Liang, 2017)	111° 11.27′	39° 21.61′	54	245	2400	MS
35(Wang, 2006)	111° 15.00′	39° 22.00′	100	787	4622	PM
36(Liu, 2020)	111° 17.14′	39° 19.05′	148	8000	7294	PM
37(Liu, 2020)	111° 15.94′	39° 18.73′	148	5800	7294	PM
38(Liu, 2020)	111° 14.67′	39° 19.57′	150	4800	7462	PM
39(Li et al., 2021)	111° 15.21′	39° 22.48′	135	3700	6530	TCN
40(Liang, 2017)	111° 20.80′	39° 45.56′	34	128	1232	MS
41(Li et al., 2021)	111° 27.00′	39° 55.42′	141	4100	6044	TCN
I(Qiu et al., 2014)	110° 27.36′	36° 04.12′	67	118.5 ± 5.6	824	OSL
II(Qiu et al., 2014)	110° 27.00′	36° 04.12′	45	93.2 ± 9.4	553	OSL
III(Qiu et al., 2014)	110° 15.36′	36° 04.48′	18	91.6 ± 5.3	428	OSL
IV(Qiu et al., 2014)	110° 09.00′	36° 01.48′	11	119.4 ± 6.7	382	OSL

* Samples from the trunk channel are marked with Arabic numbers, from tributaries with Roman numbers. MS is abbreviation of magnetic susceptibility; PM is abbreviation of paleomagnetism; OSL is abbreviation of optically stimulated luminescence. TCN is abbreviation of terrestrial cosmogenic nuclides.

landscape in the southeast, due to extensive fluvial incision and, evidently, enough rainfall to drive fluvial processes in the Loess Plateau, whereas in the northwest a vast desert dominates and westerly to northwesterly winds become the driving erosion force (Liu and Lai, 2012; Kapp et al., 2015) (Fig. 1A).

2.2. Proposed integration history in the middle Yellow River

Previous studies have mainly hypothesized three exclusive integration processes in the middle Yellow River. The first proposes that the Yellow River was an eastward-draining river that flowed directly across the Weihe Graben to the lower reach (Fig. 3A). In this hypothesis, the square bend around the Ordos Block is thought to have developed in response to the late Miocene-early Pliocene tectonic uplift in the northeastern Tibetan Plateau and associating subsidence around the Ordos Block (Lin et al., 2001; Liu, 2020). Stratigraphic sections and imbrication of pebbles are taken as the main evidences to support the idea (Lin et al., 2001).

The second proposes that there were paleolakes in the Hetao and Weihe Grabens (Fig. 3B), and the paleolake in the Weihe Graben regressed at 0.25 Ma in response to entrenchment of the Sanmen Gorge, which induced a sudden base-level fall at the outlet of the Jinshan Gorge (Jiang et al., 2007; Liang et al., 2015). A knickpoint then emerged and has now retreated ~275 km upstream. Connection between the Jinshan Gorge and the paleolake in the Hetao Graben is suggested to have occurred at 0.1 Ma, having caused another rapid bedrock river incision in response to increased discharge (Liang et al., 2015). In this way the Yellow River developed its final configuration possibly as recently as 0.1 Ma. Ages of the fluvial-lacustrine deposits are used to support the late Pleistocene integration. No dominant driving factor is identified for the proposed integration (Liang et al., 2015, 2022).

The third proposes that the square bend developed between 3.7 and 1.2 Ma (Fig. 3C), and the main evidence provided is ages of the highest terraces along the Jinshan Gorge (Pan et al., 2012), under the assumption that these terraces were only formed after the river integration. Researchers who suggest the third hypothesis also incorporated paleolake regression in the Weihe Graben and implied that, before the entrenchment of the Sanmen Gorge, the Yellow River was blocked by the Sanmen Horst and was unable to reach the sea (Hu et al., 2017). The proposed early Pleistocene integration is suggested as a result of sea level fluctuations (Xiao et al., 2020).

2.3. Dated terraces in the trunk channel and in tributaries

Terraces in the Yellow River trunk channel with published age constraints are mainly distributed at ~70 km, ~300 km, ~480 km and ~ 600 km upstream from the gorge outlet (Fig. 1B and C, Table 1). These cross sections with several levels of dated river terraces suggest increased river incision in the past ~100 ka or ~ 250 ka from samples dated with OSL or magnetic susceptibility (MS).

However, lower terraces show ages older than higher terraces at some cross sections: at ~70 km upstream from the gorge outlet, a 2.46 Ma (TCN) terrace is ~100 m lower than terraces of ~1 Ma (PM); at ~480 km upstream, a 1.47 Ma (TCN) terrace and a 4.4 Ma (TCN) terrace are lower than terraces of 1.24 Ma (PM) and 3.3 Ma (PM), respectively.

Studies of terraces in tributaries along the gorge are much more limited (Fig. 1B and C, Table 1). River terraces in the Shiwanghe, a tributary located ~60 km upstream from the gorge outlet, have been systematically investigated by Qiu et al. (2014) with OSL dating. These data suggest that in the past 100 ka the average incision rate in the lower reach of the Shiwanghe has been about three times higher than rates in the upstream reaches. A few other terraces have been dated by Qiu et al. (2014) within this tributary. Qiu et al. (2014) OSL-dated another terrace near the confluence with a strath height of ~13 m to 30.0 ± 4.3 ka, but suggest that this age is overestimated. Two other terraces located at ~1.8 km and ~ 15 km upstream from the confluence are dated to have been formed at 52.8 ± 3.4 ka and 32.9 ± 2.8 ka, respectively, while their strath heights are unclear.

To our knowledge, it is the only tributary along the Jinshan Gorge with constraints on its incision rate. The limited number of dated terraces from other tributaries along the gorge restricts further insights into the incision pattern on a large spatial scale.

3. Methods

A field survey was undertaken broadly on six tributaries distributed along the Jinshan Gorge to investigate the incision history (Fig. 1B). For most tributaries, roads were often not built along the channel, but on the interfluves, with rare channel crossings, which made large portions of the catchments unreachable and continuous survey along the channel unrealistic. Available cross-transects hence were mostly separated by large distances, making reliable terrace correlation very challenging.

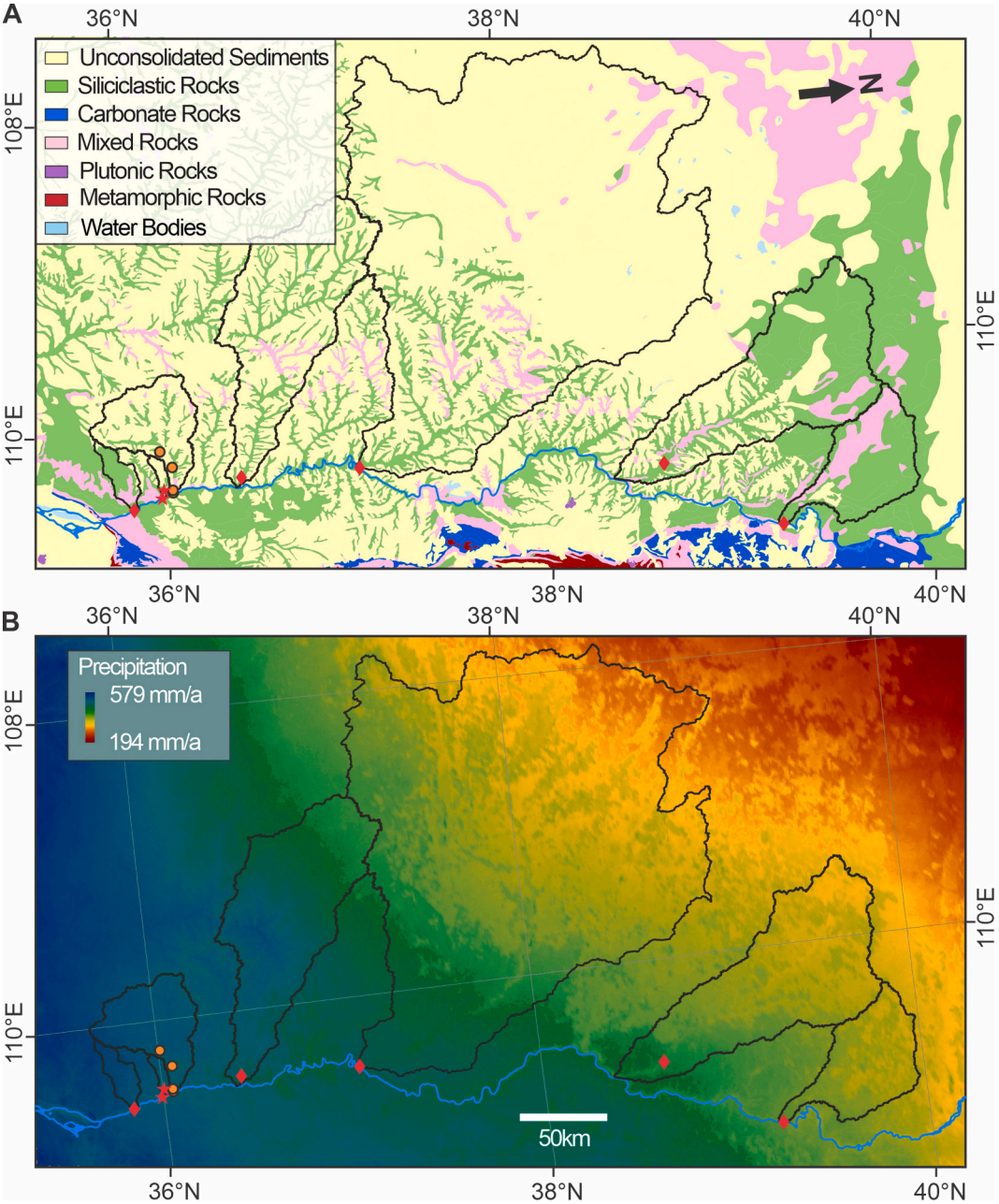

Fig. 2. Lithology and annual precipitation in study area. **(A)** Lithology of the studied tributaries. The map is derived from Global Lithological Map Database (https://www.geo.uni-hamburg.de/geologie/forschung/aquatische-geochemie/glim.html). **(B)** Annual mean precipitation of the studied tributaries. Values are estimated with precipitation data from 1970 to 2000 with 30 s resolution (http://www.worldclim.org/version2).

The terrace stratigraphy was mainly observed along road cuts. Seven cross-transects were analyzed in detailed with terrace deposits taken for terrace formation age constraints (Tables 2–4). The surveyed terraces are floored by the strath unconformity and the fill includes gravels with sandy matrix, followed by sand and silt. The transition towards the overlying aeolian deposits is locally difficult to define, given the relatively coarse-grained nature of the loess deposits, and the observed cases of interfingering of aeolian and fluvial sand and silt deposits. Pedogenic features, mostly carbonate crusts around pebbles or thin calcretes, were locally observed atop the alluvial deposits. The alternating intervals of loess-paleosol, overlying the terrace fill, were tentatively counted in the field to provide a rough minimum age estimation of the terrace formation. In fact, the pattern of loess-paleosol alternations can be correlated across the Loess Plateau and with the marine oxygen isotope stages (Liu, 1985).

Topographic surveying was done by in situ precise measurement of the elevation of the strath unconformity with respect to the modern channel, via laser distance meter. This instrument was also used to obtain the thickness of the various stratigraphic units of the alluvial fill. Differential GPS was used to obtain elevations of riverbeds and of the top of fluvial terrace gravels.

3.1. Terrace dating by luminescence

Sampling for IRSL was done following the methodology of Zhong et al. (2020). In the field, about 10 cm of surface material was removed to expose fresh deposits. Each sample was taken in a 25 cm long and 5 cm wide steel pipe with black plastic bags on both sides to shield the sample from any light exposure. Samples were collected as close as possible to the strath unconformity, in order to obtain a maximum age of

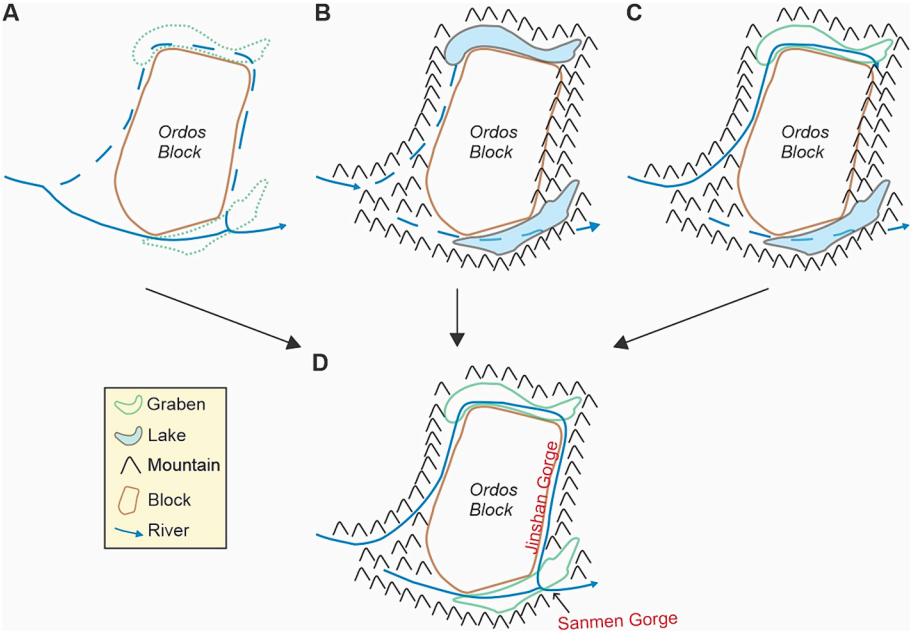

Fig. 3. Sketches for settings before hypothetical integration in the middle Yellow River. **(A)** Proposed setting before integration in late Miocene-early Pliocene by Lin et al. (2001). **(B)** Proposed setting before integration around 0.25 Ma by Liang et al. (2015). **(C)** Proposed setting before integration between 3.7 and 1.2 Ma by Pan et al. (2012) and Hu et al. (2017). **(D)** Current setting in the middle Yellow River.

Table 2
Geographic location, radioelement abundances and calculated cosmic and total (environmental) dose rates. A water content of 15 ± 5 wt% was assumed.

Sample	Longitude	Latitude	Strath height [m]	Depth [m]	K [wt%]	Th [μg/g]	U [μg/g]	$\dot{D}_{cosmic}$ [Gy/ka]	$\dot{D}_{total}$ [Gy/ka]
YH06	110°30′37.41″	35°51′29.54″	83 ± 1	10	2.27 ± 0.11	9.8 ± 0.3	2.3 ± 0.1	0.073 ± 0.007	3.859 ± 0.195
YH18	110°23′18.96″	36°26′24.34″	25.4 ± 1	8	1.92 ± 0.09	7.8 ± 0.2	2.0 ± 0.1	0.089 ± 0.009	3.391 ± 0.180
YH25	110°25′30.97″	37° 3′53.76″	36.8 ± 0.5	10	1.90 ± 0.09	9.1 ± 0.3	2.1 ± 0.1	0.074 ± 0.007	3.464 ± 0.182
YH28	110°39′2.48″	38°39′43.19″	26 ± 1	4	2.42 ± 0.12	8.7 ± 0.3	1.9 ± 0.1	0.145 ± 0.014	3.901 ± 0.198
YH33	111° 9′38.58″	39°14′35.15″	22.3 ± 0.5	13	2.03 ± 0.10	12.1 ± 0.4	2.1 ± 0.1	0.061 ± 0.006	3.750 ± 0.190

Table 3
Results of IRSL dating and estimated minimum ages. Associated marine isotope stages (MIS) are indicated in the last column.

Sample	Signal	$\dot{D}_{total}$ [Gy/ka]	$D_{e,sim}$ [Gy]	n/N	n/N_{SS}	D_0 [Gy]	Age [ka]	$2D_0$ age [ka]	MIS
YH06	IR_{50}	3.859 ± 0.195	Saturated	0.36 ± 0.04	0.24 ± 0.02	596 ± 3	Saturated	309 ± 16	8
	$pIRIR_{150}$	3.859 ± 0.195	3188 ± 687	0.64 ± 0.02	0.65 ± 0.10	825 ± 5	826 ± 183	**429 ± 22**	**11**
	$pIRIR_{290}$	3.859 ± 0.195	Saturated	0.73 ± 0.03	0.55 ± 0.07	692 ± 2	Saturated	358 ± 19	10
YH18	IR_{50}	3.391 ± 0.180	Saturated	0.35 ± 0.06	0.25 ± 0.02	434 ± 2	Saturated	256 ± 14	7
	$pIRIR_{150}$	3.391 ± 0.180	1030 ± 447	0.57 ± 0.07	0.66 ± 0.10	514 ± 1	304 ± 133	**303 ± 16**	**9**
	$pIRIR_{290}$	3.391 ± 0.180	Saturated	0.68 ± 0.06	0.56 ± 0.07	458 ± 1	Saturated	270 ± 15	8
YH25	IR_{50}	3.464 ± 0.182	Saturated	0.34 ± 0.04	0.23 ± 0.03	979 ± 5	Saturated	565 ± 30	13
	$pIRIR_{150}$	3.464 ± 0.182	3899 ± 1078	0.62 ± 0.03	0.65 ± 0.10	1174 ± 3	1126 ± 317	**678 ± 36**	**17**
	$pIRIR_{290}$	3.464 ± 0.182	Saturated	0.65 ± 0.05	0.54 ± 0.07	1122 ± 4	Saturated	648 ± 35	16
YH28	IR_{50}	3.901 ± 0.198	Saturated	0.35 ± 0.06	0.24 ± 0.02	548 ± 3	Saturated	281 ± 15	7
	$pIRIR_{150}$	3.901 ± 0.198	2052 ± 671	0.62 ± 0.08	0.66 ± 0.10	714 ± 2	526 ± 174	**366 ± 19**	**10**
	$pIRIR_{290}$	3.901 ± 0.198	Saturated	0.63 ± 0.07	0.55 ± 0.07	657 ± 2	Saturated	337 ± 18	9
YH33	IR_{50}	3.750 ± 0.190	Saturated	0.24 ± 0.04	0.24 ± 0.02	619 ± 3	Saturated	330 ± 17	8
	$pIRIR_{150}$	3.750 ± 0.190	1177 ± 706	0.51 ± 0.10	0.66 ± 0.10	788 ± 2	**314 ± 189**	420 ± 22	**9**
	$pIRIR_{290}$	3.750 ± 0.190	2269 ± 755	0.53 ± 0.11	0.55 ± 0.07	678 ± 2	605 ± 204	361 ± 19	10

Table 4
AMS ^{14}C sample information.

Sample	Longitude	Latitude	d13C/o/oo	Strath height [m]	Conventional ^{14}C age [ka BP]	Calibrated ^{14}C cal age [cal ka BP]
YH08	110°24′32.50″	36°1′32.82″	−24.9	2.8 ± 0.1	39.59 ± 0.42	43.47–42.46
YH11	110°27′34.44″	36°0′52.72″	−22.3	9.5 ± 0.5	24.10 ± 0.12	28.63–27.88

the erosional process, so we selected the lowest silt and sand bed within the gravelly unit (Shen et al., 2023). In most cases, however, the first available sandy bed was atop the gravel unit in the overbank facies.

Luminescence measurements were performed in the Institute of Earth Surface Dynamics, University of Lausanne. Because signals enter saturation at relatively low doses in quartz OSL dating of fluvial

sediments, we directly targeted K-feldspar minerals for a higher dating range. Following standard K-feldspar coarse grain sample preparation, a multi-elevated temperature (MET) post-infrared infrared stimulated luminescence (pIRIR) protocol following the protocol by Li and Li (2011), while slightly varying the IRSL stimulation temperatures, was applied to detect IRSL signals least affected by anomalous fading (see supplementary file for information on sample preparation and technical details of measurements). IRSL signals were stimulated at temperatures of 50 °C, 150 °C and 290 °C after a preheat of 300 °C (10 s) for readout of the natural, regenerated and test doses in a single-aliquot regeneration protocol. A 200 s IRSL cleanout step at 320 °C was inserted after each regeneration cycle to reduce charge carry-over to the next cycle. Up to nine multi-grain aliquots (2 mm diameter) were analyzed per sample. Fading tests were conducted on samples YH06, YH18 and YH25 by applying the same regeneration dose repeatedly, interrupted by logarithmically increased delay times between regeneration cycles (Table S1). From these measurements and following Huntley (2006) the dimensionless recombination density ρ' was derived with the function 'analyse_FadingMeasurement()', as implemented in the R-package 'Luminescence' (v0.9.10) (Kreutzer et al., 2012, 2020; Kreutzer and Burow, 2020). Dose-response was approximated by a single-saturating exponential function and corrected for anomalous fading using the average ρ' value for each signal (IR_{50}, $pIRIR_{150}$, $pIRIR_{290}$) following Kars et al. (2008), which was done using the 'calc_Huntley2006()' function (King et al., 2018; King and Burow, 2020) to derive the fading-corrected equivalent dose (D_e). Radioelement concentrations of representative and homogenized sediment samples from the surrounding of the IRSL sampling holes were determined by fusion inductively coupled plasma mass spectrometry (FUS-ICP-MS). Finally, the conversion factors of Guérin et al. (2011) together with the grain-size attenuation factors of Guérin et al. (2012) and Brennan et al. (1991) were used to calculate environmental dose rates using DRAC v1.2 (Durcan et al., 2015); further details are reported in the supplementary information.

3.2. Terrace dating by AMS radiocarbon

Charcoal fragments within fluvial sediments were sampled for AMS radiocarbon measurements to estimate the age of fills, in terraces with low strath separation. Samples were collected as close as possible to the strath unconformity, either within the gravels or in sandy beds.

Charcoal fragments were separated under binocular microscope and sent to Beta Analytic for AMS measurement. The ^{14}C ages of samples were determined with Libby's half-life (5568 years) and calibrated with the Northern Hemisphere ^{14}C calibration curve IntCal20 (Reimer et al., 2020).

3.3. Geomorphic analysis of river profiles

Within the framework of river-profile inverse modelling to infer history of rock uplift relative to base-level, a block uplift scenario (Goren et al., 2014) assumes that points along channel networks share a common uplift history. The method has been applied to analyze river profiles of tributaries along the Jinshan Gorge by Zhong et al. (2022), considering that the gorge is located in the tectonically stable Ordos Block with little evidence of interior deformation (Shi et al., 2020). Zhong et al. (2022) estimate K (erodibility) with published river terrace data on the trunk river in the Jinshan Gorge. In this paper, we estimated K using terrace data from tributaries. The main advantage of this method is that it does not require an interpolation between the reconstructed incision history at tributary outlets and a chosen location of the trunk terrace (Zhong et al., 2022).

The response time for a perturbation to propagate from the outlet of a tributary to an upstream point x can be expressed as (Whipple and Tucker, 1999; Goren et al., 2014):

$$\tau(x) = \int_0^x \frac{dx'}{C(x')} = \int_0^x \frac{dx'}{KA(x')^m S(x')^{n-1}} = \int_0^x \frac{dx'}{KA(x')^m} \quad (1)$$

A is upstream drainage area and S is channel slope. m and n are positive constants and n is assumed to be 1. For various points within a tributary, their response time from the local outlet (confluence) varies systematically (Fig. 4A). The confluence ($x = 0$) will respond immediately. The further upstream a point is, the smaller $A(x)$, and the longer the response time $\tau(x)$ will be, i.e., the later point x will incise following the new uplift rate. The instantaneous incision rate at a point x along the channel and a time t before the present, $E(x,t)$ is expressed as:

$$E(x,t) = KA(x)^m S(x,t) = KA(x)^m \frac{\partial}{\partial x} \int_t^{t+\tau(x)} U(t')dt' \quad (2)$$

To evaluate $\frac{\partial}{\partial x}\int_t^{t+\tau(x)} U(t')dt'$ we use the Leibniz integral rule following Goren et al. (2014):

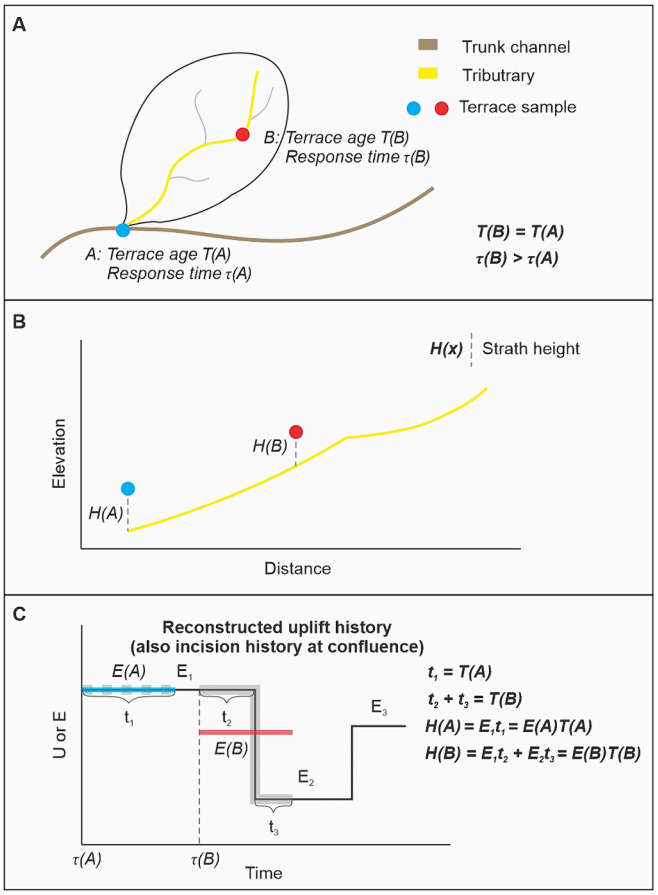

Fig. 4. Analysis method to compare terrace samples at different locations. **(A)** Terrace samples located at confluence A and upstream B of a tributary. Response time for A is smaller than response time for B so a perturbation will arrive first at A. **(B)** Schematic tributary profile with confluence A as base-level. Dashed lines show strath height for terraces at A and B. **(C)** Incision history at confluence A based on tributary profile. For any perturbation at A, there will be a delay time ($\tau(B)$) for B to react. The dashed grey line shows incision history experienced by terrace at A with age $T(A)$, and the grey line shows incision history experienced by terrace at B with age $T(B)$ ($T(B) = T(A)$). The blue line marks the average incision rate ($E(A)$) for terrace at A with age $T(A)$, and the length of the line is equal to the length of time for fluvial incision. The red line marks the average incision rate ($E(B)$) for terrace at B with age $T(B)$. Blue line and red line have equal length as $T(A) = T(B)$.

$$\frac{\partial}{\partial x}\int_{t}^{t+\tau(x)} U(t')dt' = U(t+\tau(x))\frac{d(t+\tau(x))}{dx} - U(t)\frac{dt}{dx} + \int_{t}^{t+\tau(x)} \frac{\partial U(t')}{\partial x} \quad (3)$$

In eq. 3, the first term on the right-hand side is $U(t+\tau(x))\frac{d\tau(x)}{dx}$, the second term is zero and the last term is zero (because of the block uplift assumption).

Combined eqs. 1–3, E at time t is equal to the uplift rate relative to base-level, U at time $t+\tau(x)$, i.e.,

$$E(x,t) = KA(x)^m U(t+\tau(x))\frac{d\tau(x)}{dx} = KA(x)^m U(t+\tau(x))\,(KA(x)^m)^{-1} = U(t+\tau(x)) \quad (4)$$

For a terrace with strath height $H(x)$ and age $T(x)$ (a length of time for fluvial incision) at point x (Fig. 4B), $H(x)$ is the total incision amount from time $T(x)$ to the present, and we can use eq. 4 and write:

$$H(x) = \int_0^{T(x)} E(x,t')dt' = \int_0^{T_x} U(t'+\tau(x))dt' \quad (5)$$

For the point at the confluence, its incision history is the same as uplift history, while for an upstream point, its response time must be considered when reconstructing its incision history (Fig. 4C).

We discretize the uplift rate history over j time intervals from the present $t=0$ to time t_{max} before the present: $U_1, U_2, \ldots, U_j$ are uplift rates during time intervals $\Delta t_1 = t_1 - 0$, $\Delta t_2 = t_2 - t_1, \ldots, \Delta t_j = t_j - t_{j-1}$. t_{max} is the maximal time length recorded by the river profile. For a point x, eq. 5 can be discretized as:

$$H(x) = E_l \times t_{start} + E_{l+1} \times \Delta t_{l+1} + \ldots + E_{m-1} \times \Delta t_{m-1} + E_m \times t_{end} \quad (6)$$

where E_l is equal to the uplift rate at time $\tau(x)$, $t_{start} = t_l - \tau(x)$, and $T(x) = t_{start} + \sum_{n=l+1}^{m-1}\Delta t_n + t_{end}$ (Fig. 4C). In this way, a stepwise incision history at a point x is reconstructed. The rate on average is equal to average incision rate estimated from the river terrace, but has time step information.

With a terrace data at a point x, we can obtain information of total incision amount $H(x)$ from time $T(x)$ to the present. By comparison with $H(x) - t_x^*$ plot inferred from χ-plot described in Zhong et al. (2022) (Table 1), we can estimate the value of K. In this way, scaled incision history of a drainage basin can be dimensionalized to natural units with terrace data within it, in addition to the approach described in Zhong et al. (2022), offering a complete calibration method with terrace data in any location within a river network.

In this paper, published terrace data older than ~1.2 Ma along the trunk channel, not included in Zhong et al. (2022), are incorporated to constrain K, as recent studies argue that these terraces are from the Yellow River and represent its incision history (Liu, 2020; Li et al., 2020, 2021; Xiong et al., 2022).

4. Results

4.1. General features of river terraces

Erosional remnants of river terraces were recognized and sampled in

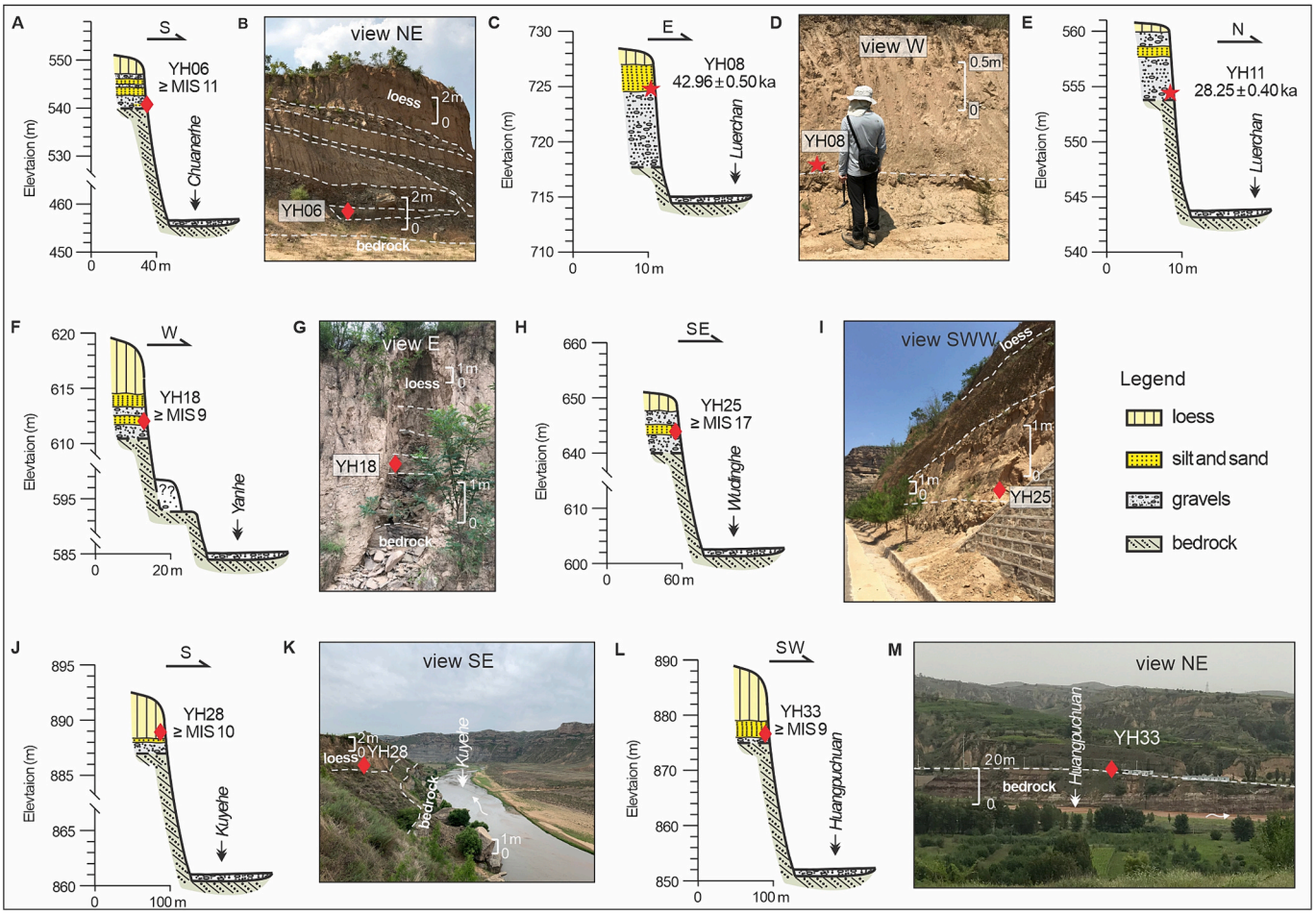

Fig. 5. Section structures and photos of the terraces of tributaries along the Jinshan Gorge. Note that the IRSL signals were overall saturated, so an age from the method can only be regarded as a minimum age (marked with "≥"). Locations of these sections and photos are shown in Fig. 1B, Tables 2 and 4. For samples YH06 and YH25, detailed field pictures are shown in Fig. S2. Note horizontal and vertical scales vary among sections.

the field. Strath terraces were observed near confluences in most tributaries. The terrace fill, overlying the strath unconformity, typically consists of 1–7 m thick gravel deposits, with closed framework and abundant sandy matrix. The measured sections were exposed by road cuts near river banks (Figs. 5 and 6). The gravels are mostly sub-rounded with an average grain size of 10–30 cm, with medium to low sphericity and a prolate trend. Locally, lenses of coarse sands and boulders up to 1 m occur (Fig. 5B). The gravels are covered by 0.5–4 m of medium-fine sand and silt, locally displaying faint parallel lamination. The fluvial deposits are covered by aeolian deposits, i.e., loess, with prominent and correlatable intervals of paleosols. Loess thickness varies from few meters in the youngest to over 10–15 m for the oldest and highest terrace (see supplementary file for details about terraces of each tributary).

Some other geomorphic features were also noticed in the field. Near the confluence with the Yellow River in the southern gorge, we observed deeply incised tributary valleys, manifesting as gorges, and the width of rivers is nearly the same as the valleyfloor (Fig. 6A). However, upstream of these tributaries, the valley-floor typically becomes several times wider than the river. In the upper reach of the Wudinghe, the valley-floor is over one kilometer wide with large floodplains (Fig. 6E), indicating weak fluvial incision. At some sites in-between, knickpoints were observed (Fig. 6B and C). In the northern reach of the Jinshan Gorge, the valley-floor at the tributary confluences is considerably greater than river width, and wide floodplains exist (Fig. 5K and M).

4.2. Terrace ages

Results from FUS-ICP-MS and determined dose rates are summarized in Table 2. Results from IRSL measurements and calculated minimum ages are given in Table 3. The level of saturation n/N as well as the field steady state (n/N_{SS}) were determined using the function 'calc_Huntley2006()' and an a-value of 0.08 ± 0.02 was assumed for all measured IRSL signals (Schmidt et al., 2018). Although finite D_e values could be determined through laboratory regenerative irradiation for some MET signals, fading-corrected IRSL dose-response curves demonstrate that all samples are close to or in dose saturation, and an example for the $pIRIR_{150}$ signal of sample YH18 is shown in Fig. S1. As expected, with an average g-value (normalized to 2 days) of 8.3 ± 0.3 %/decade, fading rates are highest for the IR_{50} signal (Thomsen et al., 2008), while the average $pIRIR_{290}$ fading rate as measured for three samples (3.3 ± 0.5 %/decade) is larger than the average $pIRIR_{150}$ fading rate (2.2 ± 0.3 %/decade) (Table S1). As a consequence, the measured natural $pIRIR_{150}$ signal is still below the field saturation ratio for most of the analyzed samples, in contrast to the IR_{50} and $pIRIR_{290}$ signals (Table 3 and Supplementary Information). Age information considered in the following is hence based on $pIRIR_{150}$ data. Additionally, given the large and asymmetric uncertainties resulting from projection of the natural IRSL signal onto the saturated part of the dose-response curve (Wintle and Murray, 2006), minimum age estimates are determined based on the D_e at $2D_0$ (of fading-corrected dose-response data), i.e., when the signal reaches $1 - e^{-2}$ (~86 %) of the saturation value, which is usually taken as the upper threshold of finite ages if a single exponential dose-response is assumed (Wintle and Murray, 2006; King et al., 2018). Considering all these uncertainties, rather than reporting numerical age estimates for these samples, we refer to Marine Isotope Stages (MIS, e.g. Gibbard and Head, 2020) to report indicative time ranges. It must be noted, anyway, that the reported luminescence age ranges correspond to minimum ages, given the overall sample saturation.

Based on IRSL measurements of sample YH06 (Figs. 1B, 5A, B, 6A and S2A), the minimum age for the formation of the high terrace in the downstream of the Chuanerhe corresponds to the MIS 11 (ca. 365–424 ka, e.g. Railsback et al., 2015). Sample YH18 yields a minimum age of MIS 9 (ca. 280–335 ka) for the formation of terrace located in the lower reach of the Yanhe (Figs. 1B, 5F and G). Terrace formation downstream of the Wudinghe is constrained to pre-date MIS 17 (ca. 675–710 ka) from sample YH25 (Figs. 1B, 5H, I and S2B). Further north, sample YH28 indicates a minimum age of terrace abandonment in the lower reach of the Kuyehe of MIS 10 (ca. 335–365 ka) (Figs. 1B, 5J and K). In the downstream of the Huangpuchuan, sample YH33 yielded a minimum age of MIS 9 (ca. 280–335 ka) for abandonment of the terrace (Figs. 1B, 5L and M).

Results from AMS ^{14}C measurements are given in Table 4. ^{14}C sample YH08 taken from the upper reaches of the Luerchuan yields an age of 43.47–42.46 cal ka BP corresponding to 2-sigma (Figs. 1B, 5C and D). In

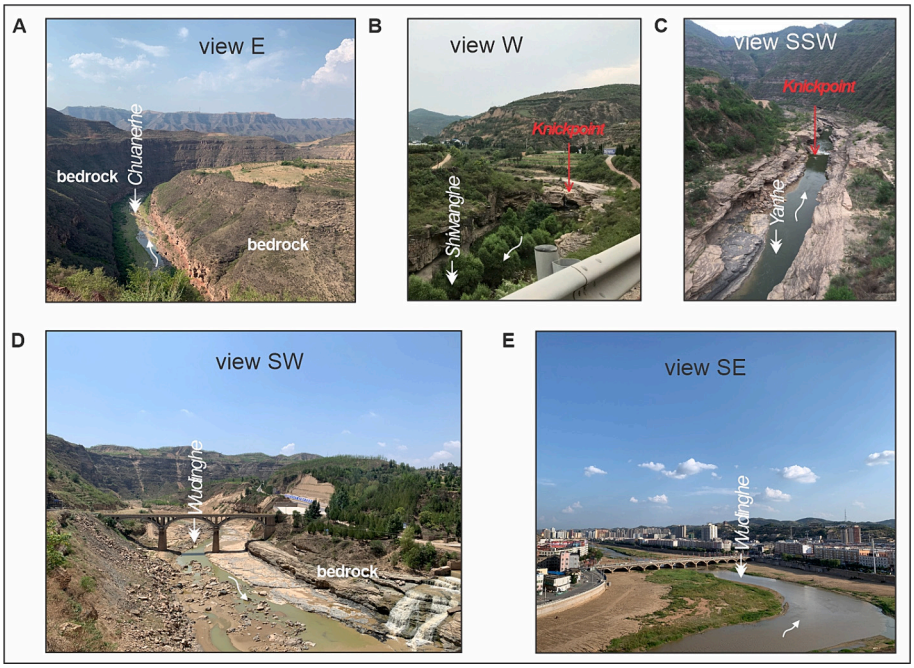

Fig. 6. Photos showing knickpoints and other landscape features of tributaries along the Jinshan Gorge. Locations of these photos are Fig. 6A (110°30′37.41″, 35°51′29.54″), Fig. 6B (110°21′34.83″, 36° 4'6.78"), Fig. 6C (110°23′18.96″, 36°26′24.34″), Fig. 6D (110°25′30.97″, 37° 3′53.76″), Fig. 6E (110°15′46.32″, 37°30′28.87″), which are also shown in Fig. 1B.

the lower reaches of the Luerchuan, the abandonment age is constrained to 28.63–27.88 cal ka BP (2-sigma) with ^{14}C sample YH11 (Figs. 1B and 5E).

4.3. Incision rates and patterns for the tributaries of the Yellow River

The incision rate is calculated by dividing strath height of a terrace by its age (Fig. 7). For IRSL dating samples except for YH33, the $2D_0$ ages shown in bold in Table 3 refer to the minimum ages and are used when calculating the incision rates. Correspondingly, the inferred incision rates obtained with the IRSL ages are maximum rates. Sample YH33 is the only sample for which the age (the third-to-last column in Table 3) is below the $2D_0$ criterion, that is why the $2D_0$ age is higher than the actual age. In this case the actual age can be seen as more reliable and should be taken for calculations of the incision rate and interpretations.

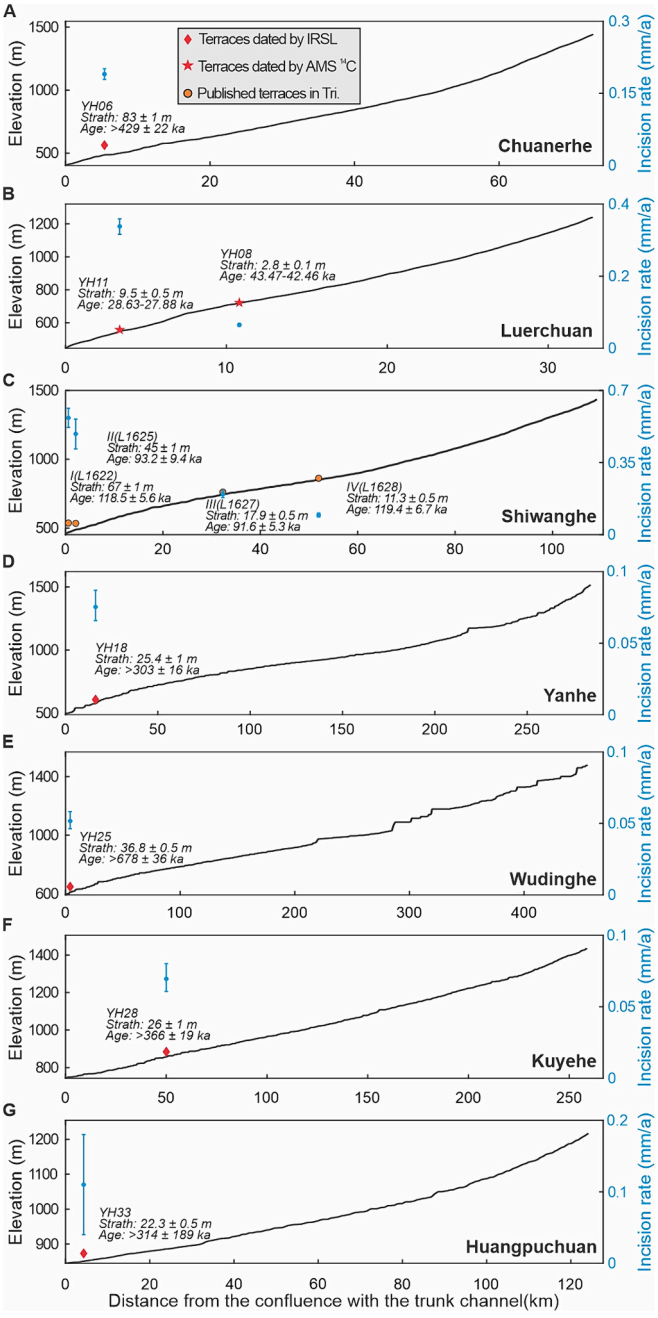

Fig. 7. Location of terraces samples in longitudinal profiles of tributaries as well as estimated incision rates. Legend of red diamonds, stars and orange circles shown in Fig. 1B. In Fig. 7C, IDs in brackets are original sample ID in Qiu et al. (2014). The blue dots show estimated average incision rates with error bar. For the X axis, left shows the downstream direction and right shows the upstream direction.

A decreasing incision rate pattern from the tributary mouth to upstream is identified in the Luerchuan (Fig. 7B): at ~3.4 km upstream from the confluence, the incision rate is estimated to be 0.34 ± 0.02 mm/a since about 28 ka, while at ~10.8 km upstream from the confluence, the estimated incision rate is only 0.06 ± 0.01 mm/a in a similar time frame. The pattern is also recognized in the Shiwanghe (Fig. 7C) investigated by Qiu et al. (2014): since ~100 ka, average incision rates are estimated to be 0.57 ± 0.04 mm/a, 0.49 ± 0.06 mm/a, 0.20 ± 0.02 mm/a and 0.09 ± 0.01 mm/a at ~0.02 km, ~2.5 km, ~33 km and ~ 54 km upstream from the confluence, respectively.

A general decreasing trend in incision rates from south to north is indicated by our terraces. In the past ~400 ka, average incision rates are estimated to be 0.19 ± 0.01 mm/a in the south (the Chuanerhe) (Figs. 1B and 7B), 0.08 ± 0.01 mm/a in the Yanhe (Figs. 1B and 7D), and 0.07 ± 0.01 mm/a in the north (the Kuyehe) (Figs. 1B, 7F and G). It may be argued that the decreasing incision rates pattern from south to north from tributary terrace data are biased by locations of samples, taken at various distance from the confluence in different tributaries. As an example, a decreasing pattern of incision rate from the confluence to upstream has been observed in the Luerchuan and the Shiwanghe. To test this, we show the reconstructed incision history for each tributary by Zhong et al. (2022), but is dimensionalized with the regional K of 1.03×10^{-5} m$^{0.3}$/a (see the following section for using this K value) (Fig. S3). Channel profile analysis indicates that all tributaries show long-term steady incision rates, but spatially the background rates generally decrease from south to north. Recently there is a clear separation of behavior with northern tributaries showing little change in incision rate, but southern tributaries indicating an increase in incision rate. These observations suggest that the decreasing incision rates to north from tributary terrace data is not due to sampling location bias.

4.4. K calibration

We compare the best-fit K values calibrated with river terrace data from tributaries and the trunk river. Parameters related to K calculation follow Zhong et al. (2022) (e.g. $m = 0.35$, $n = 1$, $A_c = 10$ km^2, $A_0 = 10$ km^2). Values of K are calibrated to be 1.03×10^{-5} m$^{0.3}$/a with all terrace data, 1.19×10^{-5} m$^{0.3}$/a with 11 terrace data in tributaries, and 0.99×10^{-5} m$^{0.3}$/a with 41 terrace data in the trunk river (Fig. 8A). The estimated K calibrated from data in tributaries is a bit larger than the K calibrated from data in the trunk river, but both K values are around ±10 % from the K calibrated with all terrace data (Fig. 8A). In addition, K values calibrated with tributary terrace data (and with all terrace data correspondingly) should be smaller considering IRSL ages we measured are the minimum ages as the signals are basically all in field saturation. Predicted ages are similar to observed terrace ages: about half of the data are predicted to within a factor of two and most of ages are predicted to within a factor of four, no matter if terrace data in the trunk or tributaries are considered (Fig. 8B), suggesting that the incision processes in tributaries and the trunk river are generally consistent. It should be noted that K was calibrated to be $2.15 \pm 0.25 \times 10^{-5}$ m$^{0.3}$/a by Zhong et al. (2022). We will discuss possible reasons for this below.

5. Discussion

5.1. Reasons for deviations from previously calibrated K

K is a function of rock strength, bed roughness and climate, where for harder bedrock and drier climate, K tends to be lower (e.g. Kirby and Whipple, 2012). K was calibrated to be $2.15 \pm 0.25 \times 10^{-5}$ m$^{0.3}$/a only with terrace data younger than ~1.2 Ma in the trunk river (Zhong et al.,

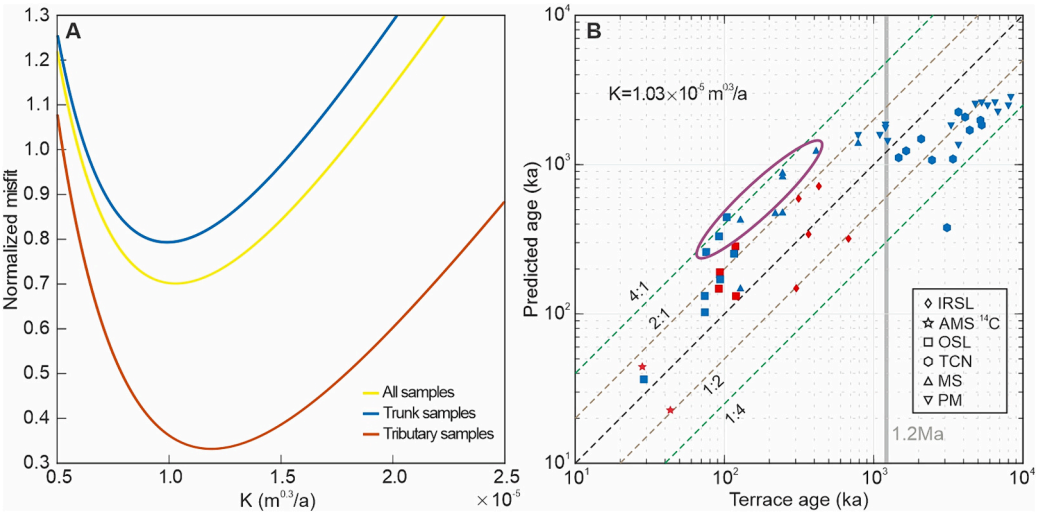

Fig. 8. Determination of *K* and Comparison between observed terrace age and predicted age. **(A)** Determination of *K* by optimization of misfit between the terrace ages and the predicted ages with the interpolated incision history (Table 1). The misfit function for all data (yellow), data in tributaries (red) and data in the trunk channel (blue). *K* values are calibrated to be 1.03 × 10^{-5} $m^{0.3}$/a with all terrace data, 1.19 × 10^{-5} $m^{0.3}$/a with only tributary terrace data, and 0.99 × 10^{-5} $m^{0.3}$/a with only trunk terrace data. **(B)** Comparison between observed terrace age and predicted age with $K = 1.03 \times 10^{-5}$ $m^{0.3}$/a calibrated with all dated terraces. Terrace data in tributaries shown in red and in the trunk channel shown in blue. Terrace ages from different dating methods shown with different shapes (see inset). Grey bar indicates dated terrace age of 1.2 Ma. Terrace data marked within a purple circle are suggested to be probably too young by this study.

2022), which is about two times larger than the *K* value estimated in this paper.

As we analyze the same area with similar lithostratigraphic units, rock strength is not supposed to change. It may be argued that the decrease in estimated *K* value is due to the fact that tributary terrace samples are included. However, the best-fit *K* values calibrated with terrace samples from tributaries and the trunk river are similar, and *K* calibrated with tributary samples is even a bit larger as described above (Fig. 8A).

Possible spatial changes in *K* values driven by precipitation variation from south to north of the Jinshan Gorge (Fig. 2B) may be proposed as a reason. However, terrace data used by both Zhong et al. (2022) and this study distribute all along the gorge, so there is no clear spatial bias in applied terrace data for *K* calibration. In addition, for a climate dominated *K* value, one would expect a decrease to the north following a northward decreasing precipitation. However, only a small improvement in fit and no northward decreasing trend in *K* values are found by grouping terrace data into lower, middle and upper segments and calculating best-fit *K* values for these subsets (Zhong et al., 2022). We thus suggest that a spatially uniform *K* is applicable in our study area and precipitation variation in space here is probably not large enough to induce significant changes in *K* values in space.

Another possible factor is long-term climate change, as older samples are considered. The *K* value is related to climatic conditions that can vary with time. The single best-fit *K* value we use actually represents average erodibility of rivers over time. Analysis of the wide loess-paleosol archive provides information on paleoclimatic variations over the Loess Plateau (e.g. Liu, 1985; Guo et al., 2002). On million-year timescale, a sustained or intensified aridity since the Pliocene, and especially after 2.6 Ma, is suggested in the Ordos Block (Fig. S4). The Asian Winter Monsoon, reflected by the > 19 μm grain-size fraction in aeolian sediments, tends to intensify, suggesting a drying trend in central Asia during the Pleistocene (Fig. S4A) (An et al., 2001). The Asian Summer Monsoon, reflected in the magnetic susceptibility index, becomes intensified, although its intensification is mostly weaker than the Winter Monsoon (Fig. S4B) (Song et al., 2007, 2014). Alternatively, sand-sized particle content from a loess section near the southern margin of the Mu Us Desert has been suggested as a more sensitive proxy for Asian Summer Monsoon intensity, which indicates stepwise weakening in Summer Monsoon strength and stepwise expansion of a desert environment at ~2.6, ~1.2, ~0.7 and ~ 0.2 Ma (Ding et al., 2005) (Fig. S4C). The long-term drying trend would yield decreasing *K* through time. In other words, if only calibrated with younger terrace data, the estimated *K* value should be smaller, which is not the case here.

As an alternative, we suggest that the deviations in calibrated *K* come from the terrace data used in our calibration. It is noteworthy that samples in the trunk river with ages younger than ~1.2 Ma, show measured terrace ages systematically younger than predicted ages, while samples older than ~1.2 Ma show measured ages mainly older than predicted ages (Fig. 8B). Assuming the prediction is correct under the assumptions of tributaries and the trunk river sharing a common incision process and of a block uplift scenario, this discrepancy could explain a larger *K* if only calibrated with younger ages in the trunk river. Therefore, a possible hypothesis is that the terraces younger than 1.2 Ma could be younger than real, due to large uncertainties associated to terrace dating. For this group of terraces, the largest difference between measured and predicted terrace ages are observed for ages of ~100 ka, constrained with OSL on quartz, and ages of ~245 ka and ~ 412 ka constrained with MS (Fig. 8B, Table 1). It should be noted that the OSL dating range on quartz is generally limited to ~50–100 ka (Faershtein et al., 2020), although strongly relying on material properties. These published ~100 ka data may underestimate real terrace ages. For samples constrained with MS, the estimated ages are mainly based on alternating intervals of loess-paleosol overlying the terrace fill, but without absolute age constraints (Hu et al., 2016) or only with OSL age constraints on upper layers of loess-paleosol intervals, rather than the contact with the alluvial deposits (Liang, 2017), which could only provide a rough minimum age estimation of the terrace formation. It is noteworthy that the considerable underestimation of OSL dating for Chinese loess samples over ~50 ka has been reported by several geochronological studies, even though that the natural quartz OSL signal is much smaller than the saturation level (Buylaert et al., 2007; Lai, 2010; Guo et al., 2012; Meng et al., 2015), which is likely caused by divergence between the laboratory- and natural-generated dose response curves (Chapot et al., 2012) and less thermal stability (Lai and Fan, 2014) for quartz OSL signals of Chinese loess samples. Terrace ages older than ~1.2 Ma are often constrained with PM and TCN burial dating (Table 1) (Fig. 8B), although it has been suggested that TCN burial ages of Yellow River's terrace deposits older than ~1 Ma are probably too old, by taking PM ages as a reference (Hu et al., 2011). We

note that studies show revised PM ages of some sections by re-correlating stratigraphic sequences (Wang et al., 2017, 2022), suggesting taking PM ages as a standard could be risky. Generally, further work in re-deciphering these PM and TCN burial ages is required, which is out of topic of this study.

The possible underestimation of OSL could explain some contrasting data from published trunk terrace samples: The largest difference in incision rates between the two groups seems to exist between ~270 km and ~ 300 km upstream from the gorge outlet, based on incision variations estimated from terrace sections along the gorge (Fig. 1C). However, no tectonic structure has been reported in-between (Zhong et al., 2022). The high incision rates at ~300 km upstream from the gorge outlet are mainly constrained with terrace ages from OSL and MS dating, which tend to provide underestimated ages, and thus overestimated incision rates. We therefore suggest that the actual change in incision rates between the two sections may not be that considerable, as indicated from the trunk terrace data.

5.2. Comparison with pseudo-terraces along the trunk middle Yellow River

Incorporating the incision recorded by the river channel profiles, Zhong et al. (2022) create an artificial geomorphic marker, named as a "pseudo-terrace", which provides a high-resolution view of spatiotemporal variation of incision rates along the Jinshan Gorge. Pseudo-terraces show higher river incision rates in the southern gorge with a recent acceleration, while the northern gorge exhibits lower and steady incision rates.

The incision patterns from terrace data in tributaries provided here are consistent with the incision variations illustrated by pseudo-terraces from channel profile modelling: the inferred recently accelerated incision rates in the southern gorge are consistent with the decreasing incision rate pattern from the tributary mouth to upstream (Fig. 7B and C) and observed knickpoints in the field (Fig. 5G and J): as the tributary mouth will respond to the recently accelerated incision rates first, whereas the further upstream, the later it will be affected by the recently accelerated incision rates due to increasing response time (Fig. 4A). In the case, the closer a river terrace to the tributary mouth, the higher the average incision rate recorded by it is supposed, as it has been influenced by the recently accelerated incision rates for a longer time, compared with the average incision rate recorded by a terrace to further upstream that only be influenced for a shorter time or even not be influenced yet (Fig. 4C). The general decreasing trend in incision rates from south to north (Fig. 6) is also consistent with the higher deduced river incision rates in the southern gorge.

It can be argued that the channel profile analysis does not provide a full view of incision history as it covers a long-time scale when climate condition definitely changes, i.e., K values would vary with time. The single best-fit K value we use actually represents average erodibility of rivers over time. Although we do not do channel profile analysis with time-varied K, climatic change impacts should affect the whole region. We thus suppose that the spatial difference from south to north would sustain.

5.3. Implications for the incision history along the Jinshan Gorge

As terrace ages >50–100 ka derived from quartz OSL dating may be underestimated (please note that we do not refer to feldspar IRSL dating here), the post ~100 ka or ~ 250 ka increased incision, derived from literature data in the trunk terraces could be unreliable, but instead, a result of dating uncertainties. The argument of dating uncertainties would challenge the decreasing incision rates to the upstream in the Shiwanghe (Figs. 1 and 6C), as the spatial pattern is constrained with OSL dating samples of ~100 ka (Qiu et al., 2014). On the other hand, from our new AMS ^{14}C terrace data in the Luerchuan, another tributary in the southern gorge (Figs. 1 and 6B), the upstream decreasing incision pattern is also observed. Furthermore, the deeply incised gorges and knickpoints observed in the downstream of southern tributaries (Fig. 5C, G and J) also support recently enhanced river incision in the southern Jinshan Gorge. Despite the exact ages of Shiwanghe terraces are probably underestimated, we suggest that the spatial pattern from them is still reliable.

Although we did not obtain multiple terrace samples along a tributary in the northern gorge to explore possible spatial changes in incision rates along the tributary, the broad valley-floors observed near northern tributaries' confluences with the trunk channel (Fig. 5P and R), contrasting to the deep gorges in the southern tributaries (Fig. 5C), suggest that increase in incision rate in the northern gorge, if existing, is much more limited.

In summary, our new incision rate data and landscape feature observations from tributaries along the gorge support a recent increase in incision rates in the southern gorge, which has been suggested both by pseudo-terraces (Zhong et al., 2022) and published river terrace data. However, incision history in the northern gorge is likely steady through time, as also indicated by pseudo-terraces (Zhong et al., 2022). Potential cause for the recent increasing incision rate in the southern Jinshan Gorge has been suggested as upper mantle processes (Zhong et al., 2022), especially a low velocity anomaly of the upper mantle beneath the southeastern and southwestern Ordos Block (Yu and Chen, 2016; Guo and Chen, 2017). The recently accelerated incision rates in the northern gorge inferred from published trunk river terraces are possibly related to large uncertainties in terrace dating.

5.4. Implications for the integration in the middle Yellow River

In the southern Jinshan Gorge, steepening of tributary profiles in their lower reaches near confluences with the trunk river (Fig. 6A-D) together with observed knickpoints (Fig. 5G and J) manifest the lower reaches as knickzones. Combined with quantitative analysis of the tributary profiles by Zhong et al. (2022), the increased incision rate in the southern gorge was sustained for several hundred thousand years (Fig. S4). This feature indicates a long-lived base-level fall at the outlet of the Jinshan Gorge, which is not compatible with a single episode of base-level fall due to a hypothetical paleo-lake regression in the Weihe Graben (Fig. 3B and C), as such an event would have only induced a short-lived pulse of incision rate.

For the hypothetical integration with the Hetao Graben (Fig. 3B), enhanced incision rates following such an event would have affected the entire Jinshan Gorge, and would have had the largest effect at the hypothesized former drainage divide in the northern gorge. However, our landscape feature observations provided here and channel profile modelling (Zhong et al., 2022) suggest incision rates in the northern gorge have been steady through the time. In addition, incision rates appear higher in the southern Jinshan Gorge, no matter if reconstructed from our new tributary terrace studies or from channel profile modelling (Zhong et al., 2022).

We acknowledge that our channel profile modelling results are based on some assumptions, like n =1 and a block uplift scenario, which probably do not provide a full view of incision history along the Jinshan Gorge. However, it should be noted that we also combine new terrace data and landscape feature observations from tributaries in our analysis. In addition, inferred quartz OSL ages of ~100 ka may be underestimated has been independently suggested by several chronologic studies (Buylaert et al., 2007; Lai, 2010; Guo et al., 2012; Meng et al., 2015). We thus posit that our implications for reasons for deviations from previously calibrated K and following the incision history along the Jinshan Gorge are mostly reliable.

In summary, we suggest that previously proposed large-scaled Pleistocene river integration in the middle Yellow River unlikely took place. If any integration occurred in the middle reach, it would have been either local or older (Xiong et al., 2022).

6. Conclusions

In this study we provide new incision rate data and landscape feature observations from six tributaries along the Jinshan Gorge in the middle Yellow River, which highlight spatially heterogeneous incision variations along the gorge: increasing incision rates towards the confluence with the trunk river in the southern Jinshan Gorge, as well as north to south increasing incision rates along the gorge are found from coeval tributary terraces. In addition, a novel method to assemble terrace data of various ages and locations is introduced. From our analysis of terrace ages derived from different dating methods, we suggest that the ~100 ka or ~ 250 ka accelerated incision in the northern gorge has most likely not occurred, but is related to the large uncertainties in terrace ages associated with OSL. This explanation can also mitigate the mismatch of incision history recorded by pseudo-terraces and river terraces along the gorge. The incision history reconstructed here further suggests that the large-scaled Pleistocene river integration in the middle Yellow River proposed previously are unlikely to have been responsible for recent incision. We suggest a re-examination of published terrace ages, which may help unravel the mysterious evolution history of the middle Yellow River.

CRediT authorship contribution statement

Yuezhi Zhong: Writing – original draft, Visualization, Validation, Resources, Methodology, Investigation, Funding acquisition, Formal analysis, Data curation, Conceptualization. **Vincenzo Picotti:** Writing – review & editing, Validation, Supervision, Project administration, Investigation, Formal analysis, Data curation, Conceptualization. **Jianguo Xiong:** Writing – review & editing, Validation, Resources, Investigation, Funding acquisition, Formal analysis, Data curation, Conceptualization. **Sean D. Willett:** Writing – review & editing, Validation, Supervision, Resources, Project administration, Methodology, Investigation, Formal analysis, Conceptualization. **Christoph Schmidt:** Writing – review & editing, Validation, Methodology, Investigation, Formal analysis, Data curation. **Georgina King:** Writing – review & editing, Validation, Investigation, Formal analysis, Data curation.

Declaration of competing interest

The authors declare no competing interest.

Data availability

Digital elevation model (DEM) data are available from the USGS Earth Explorer (https://earthexplorer.usgs.gov/). Annual mean precipitation data are available from WorldClim (http://www.worldclim.org/version2). Extended data figures and tables can be found in the supporting information.

Acknowledgments

We thank Liran Goren for discussion, Zifa Ma and Kang Liu for field assistance, and Micaela Faria for lab work assistance. This work was jointly supported by the National Natural Science Foundation of China (Grant 42488201) and the Second Tibetan Plateau Scientific Expedition and Research Program (STEP, Grant No. 2019QZKK0704). Yuezhi Zhong is supported by China Scholarship Council (Grant 201706010407).

Appendix A. Supplementary data

Supplementary data to this article can be found online at https://doi.org/10.1016/j.geomorph.2024.109330.

References

An, Z., Kutzbatch, J.E., Prell, W.L., Porder, S.C., 2001. Evolution of Asian monsoons and phased uplift of the Himalaya-Tibetan plateau since Late Miocene times. Nature 411, 62–66.

Brennan, B.J., Lyons, R.G., Phillips, S.W., 1991. Attenuation of alpha particle track dose for spherical grains. Int. J. Radiat. Appl. Instrumentation. Part D. Nucl. Tracks Radiat. Meas. 18, 249–253.

Burbank, D.W., Anderson, R.S., 2011. Tectonic Geomorphology. John Wiley & Sons.

Buylaert, J.-P., Vandenberghe, D., Murray, A.S., Huot, S., De Corte, F., Van den Haute, P., 2007. Luminescence dating of old (> 70 ka) Chinese loess: a comparison of single-aliquot OSL and IRSL techniques. Quat. Geochronol. 2, 9–14.

Cao, X., 2012. Low-level River Terraces and Loess Deposits of Typical Profile from Heiyukou to Zhangjiawan in the Middle Reach of the Yellow River. Master Thesis. Southwest Univ.

Chapot, M.S., Roberts, H.M., Duller, G.A.T., Lai, Z.P., 2012. A comparison of natural- and laboratory-generated dose response curves for quartz optically stimulated luminescence signals from Chinese Loess. Radiat. Meas. 47, 1045–1052. https://doi.org/10.1016/j.radmeas.2012.09.001.

Clinkscales, C., Kapp, P., Thomson, S., Wang, H., Laskowski, A., Orme, D.A., Pullen, A., 2021. Regional Exhumation and Tectonic History of the Shanxi Rift and Taihangshan, North China. Tectonics 40, 1–36 (e2020TC006416).

Ding, Z.L., Derbyshire, E., Yang, S.L., Sun, J.M., Liu, T.S., 2005. Stepwise expansion of desert environment across northern China in the past 3.5 Ma and implications for monsoon evolution. Earth Planet. Sci. Lett. 237, 45–55. https://doi.org/10.1016/j.epsl.2005.06.036.

Durcan, J.A., King, G.E., Duller, G.A.T., 2015. DRAC: Dose Rate and Age Calculator for trapped charge dating. Quat. Geochronol. 28, 54–61.

Faershtein, G., Porat, N., Matmon, A., 2020. Extended-range luminescence dating of quartz and alkali feldspar from aeolian sediments in the eastern Mediterranean. Geochronology 2, 101–118. https://doi.org/10.5194/gchron-2-101-2020.

Fox, M., Goren, L., May, D.A., Willett, S.D., 2014. Inversion of fluvial channels for paleorock uplift rates in Taiwan. J. Geophys. Res. Earth Surf. 119, 1853–1875. https://doi.org/10.1002/2014JF003196.

Gibbard, P.L., Head, M.J., 2020. The quaternary period. In: Geologic Time Scale 2020. Elsevier, pp. 1217–1255.

Goren, L., Fox, M., Willett, S.D., 2014. Tectonics from fluvial topography using formal linear inversion: theory and applications to the Inyo Mountains, California. J. Geophys. Res. F Earth Surf. 119, 1651–1681. https://doi.org/10.1002/2014JF003079.

Guérin, G., Mercier, N., Adamiec, G., 2011. Dose-rate conversion factors: update. Ancient TL 29, 5–8.

Guérin, G., Mercier, N., Nathan, R., Adamiec, G., Lefrais, Y., 2012. On the use of the infinite matrix assumption and associated concepts: a critical review. Radiat. Meas. 47, 778–785.

Guo, Z., Chen, Y.J., 2017. Mountain building at northeastern boundary of Tibetan Plateau and craton reworking at Ordos block from joint inversion of ambient noise tomography and receiver functions. Earth Planet. Sci. Lett. 463, 232–242. https://doi.org/10.1016/j.epsl.2017.01.026.

Guo, Z., Ruddiman, W.F., Hao, Q., Wu, H., Qiao, Y., Zhu, R., Peng, S., Wei, J., Yuan, B., Liu, T., 2002. Onset of Asian desertification by 22 Myr ago inferred from loess deposits in China. Nature 416, 159–163.

Guo, Y., Zhang, J., Qiu, W., Hu, G., Zhuang, M., Zhou, L., 2012. Luminescence dating of the Yellow River terraces in the Hukou area, China. Quat. Geochronol. 10, 129–135. https://doi.org/10.1016/j.quageo.2012.03.002.

Hu, X., Kirby, E., Pan, B., Granger, D.E., Su, H., 2011. Cosmogenic burial ages reveal sediment reservoir dynamics along the Yellow River, China. Geology 39, 839–842. https://doi.org/10.1130/G32030.1.

Hu, Z., Pan, B., Guo, L., Vandenberghe, J., Liu, X., Wang, J., Fan, Y., Mao, J., Gao, H., Hu, X., 2016. Rapid fluvial incision and headward erosion by the Yellow River along the Jinshaan gorge during the past 1.2 Ma as a result of tectonic extension. Quat. Sci. Rev. 133, 1–14. https://doi.org/10.1016/j.quascirev.2015.12.003.

Hu, Z., Pan, B.T., Bridgland, D., Vandenberghe, J., Guo, L.Y., Fan, Y.L., Westaway, R., 2017. The linking of the upper-middle and lower reaches of the Yellow River as a result of fluvial entrenchment. Quat. Sci. Rev. 166, 324–338. https://doi.org/10.1016/j.quascirev.2017.02.026.

Huntley, D.J., 2006. An explanation of the power-law decay of luminescence. J. Phys. Condens. Matter 18, 1359.

Jiang, F., Fu, J., Wang, S., Sun, D., Zhao, Z., 2007. Formation of the Yellow River, inferred from loess-palaeosol sequence in Mangshan and lacustrine sediments in Sanmen Gorge, China. Quat. Int. 175, 62–70. https://doi.org/10.1016/j.quaint.2007.03.022.

Kapp, P., Pullen, A., Pelletier, J.D., Russell, J., Goodman, P., Cai, F., 2015. From dust to dust: Quaternary wind erosion of the Mu Us Desert and Loess Plateau, China. Geology 43, 835–838. https://doi.org/10.1130/G36724.1.

Kars, R.H., Wallinga, J., Cohen, K.M., 2008. A new approach towards anomalous fading correction for feldspar IRSL dating—tests on samples in field saturation. Radiat. Meas. 43, 786–790.

King, G.E., Burow, C., 2020. Calc_Huntley2006 ( ): Apply the Huntley (2006) model, Function version 0.4.1. Lumin. Compr. Lumin. Dating Data Anal. In: Kreutzer, S., Burow, C., Dietz, M., Fuchs, M.C., Schmidt, C., Fischer, M., Friedrich, J. (Eds.), R Packag. version 0.9.10, available https//CRAN. R-project. org/package= Lumin.

King, G.E., Burow, C., Roberts, H.M., Pearce, N.J.G., 2018. Age determination using feldspar: evaluating fading-correction model performance. Radiat. Meas. 119, 58–73.

Kirby, E., Whipple, K.X., 2012. Expression of active tectonics in erosional landscapes. J. Struct. Geol. 44, 54–75. https://doi.org/10.1016/j.jsg.2012.07.009.
Kreutzer, S., Burow, C., 2020. analyse_FadingMeasurement ( ): analyse fading measurements and returns the fading rate per decade (g-value). Function version 0.1. 15. Lumin. In: Kreutzer, S., Burow, C., Dietze, M., Fuchs, M.C., Schmidt, C., Fischer, M., Friedrich, J. (Eds.), Compr. Lumin. Dating Data Anal. R Packag. version 0.9.10. https://CRAN.R-project.org/package=Luminescence.
Kreutzer, S., Schmidt, C., Fuchs, M.C., Dietze, M., Fischer, M., Fuchs, M., 2012. Introducing an R package for luminescence dating analysis. Ancient TL 30, 1–8.
Kreutzer, S., Burow, C., Dietze, M., Fuchs, M., Schmidt, C., Fischer, M., Friedrich, J., Riedesel, S., Autzen, M., Mittelstrass, D., 2020. Luminescence: Comprehensive Luminescence Dating Data Analysis. R Package Version 0.9.10. https://CRAN.R-project.org/package=Luminescence.
Lai, Z., 2010. Chronology and the upper dating limit for loess samples from Luochuan section in the Chinese Loess Plateau using quartz OSL SAR protocol. J. Asian Earth Sci. 37, 176–185. https://doi.org/10.1016/j.jseaes.2009.08.003.
Lai, Z., Fan, A., 2014. Examining quartz OSL age underestimation for loess samples from Luochuan in the Chinese loess plateau. Geochronometria 41, 57–64. https://doi.org/10.2478/s13386-013-0138-1.
Li, B., Li, S.H., 2011. Luminescence dating of K-feldspar from sediments: a protocol without anomalous fading correction. Quat. Geochronol. 6, 468–479. https://doi.org/10.1016/j.quageo.2011.05.001.
Li, T., Liu, F., Abels, H.A., You, C., Zhang, Z., Chen, J., Ji, J., Li, Laifeng, Li, Le, Liu, H., Ren, C., Xia, R., Zhao, L., Zhang, W., Li, G., 2017. Continued obliquity pacing of East Asian summer precipitation after the mid-Pleistocene transition. Earth Planet. Sci. Lett. 457, 181–190. https://doi.org/10.1016/j.epsl.2016.09.045.
Li, Z., Zhang, K., Liang, H., Chen, Zhen, Li, X., Khan, W., Yu, Z., Chen, Zihao, Huang, P., 2020. Initial incision of the Jinshan Gorge of the Yellow River, China, constrained by terrestrial in situ cosmogenic nuclides chronology. Quat. Int. 550, 111–119. https://doi.org/10.1016/j.quaint.2020.03.047.
Li, Z., Zhang, K., Liang, H., Chen, Z., Ma, Z., Xiong, J., Huang, P., 2021. Large river chronology along the Jinshaan Gorge on the Yellow River and its implications for initialization. Geomorphology 400, 108092. https://doi.org/10.1016/j.geomorph.2021.108092.
Liang, H., 2017. Long-term Fluvial Evolution and Response to Basin Connection along the Jinshan-Sanmen Gorge, Yellow River since Late Mid-Pleistocene. Ph. D. Thesis. Sun Yat-Sen Univ.
Liang, H., Zhang, K., Fu, J., Li, L., Chen, J., Li, S., Chen, L., 2015. Bedrock river incision response to basin connection along the Jinshan Gorge, Yellow River, North China. J. Asian Earth Sci. 114, 203–211. https://doi.org/10.1016/j.jseaes.2015.07.010.
Liang, H., Zhang, K., Li, Zhongyun, Fu, J., Yu, Z., Xiong, J., Li, X., Ma, Z., Huang, P., Li, Zhigang, 2022. How headward erosion breaches upstream paleolakes: Insights from dated longitudinal fluvial terrace correlations within the Sanmen Gorge, Yellow River. GSA Bull. 135, 1602–1617.
Lin, A., Yang, Z., Sun, Z., Yang, T., 2001. How and when did the Yellow River develop its square bend ? Geology 951–954.
Liu, D., 1985. Loess and the Environment. Science Press.
Liu, Y., 2014. Magnetostratigraphy of red clay and silt layer of Qiujiayan Section, Shenmu county and its implications to the formation of the Yellow River. J. Anqing Teach. Coll. (Natural Sci. Ed.) 20, 115–120.
Liu, Y., 2020. Neogene fluvial sediments in the northern Jinshaan Gorge, China: Implications for early development of the Yellow River since 8 Ma and its response to rapid subsidence of the Weihe-Shanxi Graben. Palaeogeogr. Palaeoclimatol. Palaeoecol. 546, 109675 https://doi.org/10.1016/j.palaeo.2020.109675.
Liu, K., Lai, Z.P., 2012. Chronology of Holocene sediments from the archaeological Salawusu site in the Mu Us Desert in China and its palaeoenvironmental implications. J. Asian Earth Sci. 45, 247–255. https://doi.org/10.1016/j.jseaes.2011.11.002.
Liu, Y., Li, Y., Lu, H., Si, S., Zhao, H., 2007. Preliminary study of alluvial pebbles on high terraces of the Yellow River from Baode to Kehu in Shanxi-Shaanxi Gorge. Acta Sci. Nat. Univ. Pekin. 43, 808–815.
Meng, Y., Zhang, J., Qiu, W., Fu, X., Guo, Y., Zhou, L., 2015. Quaternary geochronology optical dating of the Yellow River terraces in the Mengjin area (China). First results 30, 219–225. https://doi.org/10.1016/j.quageo.2015.03.006.
Merritts, D.J., Vincent, K.R., Wohl, E.E., 1994. Long river profiles, tectonism, and eustasy: a guide to interpreting fluvial terraces. J. Geophys. Res. Solid Earth 99, 14031–14050.
Pan, B., Hu, Z., Wang, J., Vandenberghe, J., Hu, X., Wen, Y., Li, Q., Cao, B., 2012. The approximate age of the planation surface and the incision of the Yellow River. Palaeogeogr. Palaeoclimatol. Palaeoecol. 356–357, 54–61. https://doi.org/10.1016/j.palaeo.2010.04.011.
Pazzaglia, F.J., Gardner, T.W., Merritts, D.J., 1998. Bedrock fluvial incision and longitudinal profile development over geologic time scales determined by fluvial terraces. Geophys. Monogr. Geophys. Union 107, 207–236.
Qiu, W.L., Zhang, J.F., Wang, X.Y., Guo, Y.J., Zhuang, M.G., Fu, X., Zhou, L.P., 2014. The evolution of the Shiwanghe River valley in response to the Yellow River incision in the Hukou area, Shaanxi, China. Geomorphology 215, 34–44. https://doi.org/10.1016/j.geomorph.2014.01.011.
Railsback, L.B., Gibbard, P.L., Head, M.J., Voarintsoa, N.R.G., Toucanne, S., 2015. An optimized scheme of lettered marine isotope substages for the last 1.0 million years, and the climatostratigraphic nature of isotope stages and substages. Quat. Sci. Rev. 111, 94–106.
Reimer, P.J., Austin, W.E.N., Bard, E., Bayliss, A., Blackwell, P.G., Bronk Ramsey, C., Butzin, M., Cheng, H., Edwards, R.L., Friedrich, M., Grootes, P.M., Guilderson, T.P., Hajdas, I., Heaton, T.J., Hogg, A.G., Hughen, K.A., Kromer, B., Manning, S.W., Muscheler, R., Palmer, J.G., Pearson, C., Van Der Plicht, J., Reimer, R.W., Richards, D.A., Scott, E.M., Southon, J.R., Turney, C.S.M., Wacker, L., Adolphi, F., Büntgen, U., Capano, M., Fahrni, S.M., Fogtmann-Schulz, A., Friedrich, R., Köhler, P., Kudsk, S., Miyake, F., Olsen, J., Reinig, F., Sakamoto, M., Sookdeo, A., Talamo, S., 2020. The IntCal20 northern hemisphere radiocarbon age calibration curve (0-55 cal kBP). Radiocarbon 62, 725–757. https://doi.org/10.1017/RDC.2020.41.
Rhoads, B.L., 2020. River Dynamics: Geomorphology to Support Management. Cambridge University Press.
Ritts, B.D., Weislogel, A., Graham, S.A., Darby, B.J., 2009. Mesozoic tectonics and sedimentation of the giant polyphase nonmarine intraplate Ordos Basin, Western North China Block. Int. Geol. Rev. 51, 95–115. https://doi.org/10.1080/00206810802614523.
Roberts, G.G., White, N., 2010. Estimating uplift rate histories from river profiles using African examples. J. Geophys. Res. Solid Earth 115, 1–24. https://doi.org/10.1029/2009JB006692.
Schmidt, C., Bösken, J., Kolb, T., 2018. Is there a common alpha-efficiency in polymineral samples measured by various infrared stimulated luminescence protocols? Geochronometria 45, 160–172.
Shen, Q., Zhou, Y., Xu, Y., Lai, Y., Yan, X., Huang, X., Liu, X., Zhong, J., Zhu, S., Li, Z., Lai, Z., 2023. Late Quaternary river evolution and its response to climate changes in the upper Mekong River of the Qinghai–Tibetan Plateau. Geomorphology 442, 108920. https://doi.org/10.1016/j.geomorph.2023.108920.
Shi, W., Dong, S., Hu, J., 2020. Neotectonics around the Ordos Block, North China: a review and new insights. Earth-Science Rev. 200, 102969 https://doi.org/10.1016/j.earscirev.2019.102969.
Song, Y., Fang, X., Torii, M., Ishikawa, N., Li, J., An, Z., 2007. Late Neogene rock magnetic record of climatic variation from Chinese eolian sediments related to uplift of the Tibetan Plateau. J. Asian Earth Sci. 30, 324–332. https://doi.org/10.1016/j.jseaes.2006.10.004.
Song, Y., Fang, X., King, J.W., Li, J., Naoto, I., An, Z., 2014. Magnetic parameter variations in the Chaona loess/paleosol sequences in the central Chinese Loess Plateau, and their significance for the middle Pleistocene climate transition. Quat. Res. 81, 433–444. https://doi.org/10.1016/j.yqres.2013.10.002.
Thomsen, K.J., Murray, A.S., Jain, M., Bøtter-Jensen, L., 2008. Laboratory fading rates of various luminescence signals from feldspar-rich sediment extracts. Radiat. Meas. 43, 1474–1486.
Wang, J., 2006. Formation and Evolution of the Middle Reaches of the Yellow River since Late Cenozoic. Ph. D.. Thesis Lanzhou Univ.
Wang, W., Zheng, W., Zhang, P., Li, Q., Kirby, E., Yuan, D., Zheng, D., Liu, C., Wang, Z., Zhang, H., Pang, J., 2017. Expansion of the Tibetan Plateau during the Neogene. Nat. Commun. 8 https://doi.org/10.1038/ncomms15887.
Wang, W., Zhang, P., Garzione, C.N., Liu, C., Zhang, Z., Pang, J., Wang, Y., Zheng, D., Zheng, W., Zhang, H., 2022. Pulsed rise and growth of the Tibetan Plateau to its northern margin since ca. 30 Ma. Proc. Natl. Acad. Sci. USA 119, 1–8. https://doi.org/10.1073/pnas.2120364119.
Whipple, K.X., Tucker, G.E., 1999. Dynamics of the stream-power river incision model: implications for height limits of mountain ranges, landscape response timescales, and research needs. J. Geophys. Res. Solid Earth 104, 17661–17674. https://doi.org/10.1029/1999JB900120.
Willett, S.D., McCoy, S.W., Taylor Perron, J., Goren, L., Chen, C.Y., 2014. Dynamic reorganization of River Basins. Science 80, 343. https://doi.org/10.1126/science.1248765.
Wintle, A.G., Murray, A.S., 2006. A review of quartz optically stimulated luminescence characteristics and their relevance in single-aliquot regeneration dating protocols. Radiat. Meas. 41, 369–391.
Xiao, G., Sun, Y., Yang, J., Yin, Q., Dupont-Nivet, G., Licht, A., Kehew, A.E., Hu, Y., Geng, J., Dai, G., Zhao, Q., Wu, Z., 2020. Early Pleistocene integration of the Yellow River I: Detrital-zircon evidence from the North China Plain. Palaeogeogr. Palaeoclimatol. Palaeoecol. 546 https://doi.org/10.1016/j.palaeo.2020.109691.
Xiong, L., Tang, G., 2019. Loess Landform Inheritance: Modeling and Discovery. Springer.
Xiong, J., Liu, Y., Zhang, P., Deng, C., Picotti, V., 2022. Entrenchment of the Yellow River since the late Miocene under changing tectonics and climate. Geomorphology 416, 108428. https://doi.org/10.1016/j.geomorph.2022.108428.
Yu, Y., Chen, Y.J., 2016. Seismic anisotropy beneath the southern Ordos block and the Qinling-Dabie orogen, China: Eastward Tibetan asthenospheric flow around the southern Ordos. Earth Planet. Sci. Lett. 455, 1–6.
Zhang, J.F., Wang, X.Q., Qiu, W.L., Shelach, G., Hu, G., Fu, X., Zhuang, M.G., Zhou, L.P., 2011. The paleolithic site of Longwangchan in the middle Yellow River, China: chronology, paleoenvironment and implications. J. Archaeol. Sci. 38, 1537–1550. https://doi.org/10.1016/j.jas.2011.02.019.
Zhong, Y., Xiong, J., Li, Y., Zheng, W., Zhang, P., 2020. Constraining late Quaternary crustal shortening in the Eastern Qilian Shan from deformed river terraces. J. Geophys. Res. Solid Earth 1–17. https://doi.org/10.1029/2020JB020631.
Zhong, Y., Willett, S.D., Picotti, V., Xiong, J., Zhang, H., 2022. Spatial and temporal variations of incision rate of the middle Yellow River and its tributaries. J. Geophys. Res. Earth Surf. 1–15 https://doi.org/10.1029/2021jf006327.